Anisotropic Viscous Flow Simulation in Abaqus

Anthony J. Favaloro, Drew E. Sommer, and R. Byron Pipes

School of Aeronautics and Astronautics, Purdue University, West Lafayette, IN, US

***Abstract**: The flow behavior of fiber filled material systems is of interest in polymeric composites processing. Specifically, applications such as injection molding and compression molding are concerned with determining the final fiber orientation state. As applications move towards increased fiber length and volume fractions seeking enhanced mechanical performance, significant anisotropy is introduced in the viscous response during processing. However, commercially available tools for molding simulation do not account for strongly coupled anisotropic flow. A method is presented in which Abaqus/Standard and Abaqus/Explicit are utilized to perform coupled anisotropic viscous flow simulation and fiber orientation analysis using a developed UMAT and VUMAT respectively. Hybrid elements are utilized in Abaqus/Standard to solve simple flow problems such as squeeze flow, while the smoothed particle hydrodynamics method is utilized in Abaqus/Explicit to solve flow problems into complex geometries. The anisotropic, viscous constitutive model is presented along with implementation details for both the UMAT and VUMAT. Select results are presented which highlight the effects introduced by considering a coupled flow analysis including validation results for squeeze flow using Abaqus/Standard and center gated disk flow using Abaqus/Explicit.*

***Keywords**: Abaqus, Abaqus/Standard, Abaqus/Explicit, UMAT, VUMAT, user subroutines, anisotropic viscosity, fiber orientation, composite materials, composites, viscous flow.*

1. Introduction

The addition of reinforcing fibers into polymeric materials for use in injection molding and compression molding is a common practice to add stiffness and strength to molded parts. For structural applications in both aerospace and automotive, stiffness, strength, and weight requirements are pushing towards the use of long carbon fibers at large volume fractions. When using these material systems in a molding process, the final fiber orientation state of the part is important to understand as the fiber orientation state directly affects the performance.

The response of fibers suspended in a viscous fluid is a relatively well-understood phenomenon. The response of a single ellipsoid surrounded by an infinite viscous fluid was solved for in 1922 by Jeffery (Jeffery, 1922). Extending this work to semi-concentrated suspensions of fibers, Folgar and Tucker added an isotropic rotary diffusion term to account for fiber-fiber interactions (Folgar, 1984). Advani and Tucker introduced the use of orientation tensor to reduce the number of independent variables required per integration point from upwards of 400 to 5 (Advani, 1987). However, this reduction also introduced a closure problem in that the second order orientation tensor cannot be updated without higher order orientation tensor information leading to the requirement for approximate orientation tensor update methods. More recent advancements such as the anisotropic rotary diffusion with reduced strain closure model (Phelps, 2009) and the improved anisotropic rotary diffusion with retarding principal rate model (Tseng, 2016) seek to account for the effects of long fibers through the addition of anisotropic orientation diffusion schemes.

These theories have generally been applied in the absence of a constitutive model that couples the determined fiber orientation to the response of the effective fluid. Early studies considering the necessity of a coupled approach for injection molding applications of short fibers concluded the effects were negligible (Tucker, 1991). However, Ericsson et al. (Ericsson, 1997) displayed the necessity a coupled solution through both experimentation and a simple model in the case of squeeze flow of an initially circular disk with an initial orientation state that is has preferential alignment. The initially circular disks were found to deform into ellipses with axis ratios dependent on the orientation state.

In this work, we have built a platform for coupled fiber orientation and anisotropic viscous flow analysis within both Abaqus/Standard and Abaqus/Explicit through a UMAT and VUMAT respectively.

2. Method Description

When discussing a fiber reinforced system, we must understand that a straight fiber, being a transversely isotropic geometry, requires only a single orientation to fully describe. We will denote an orientation as a vector p_i with $p_i p_i = 1$ with repeated indices representing summation which could equivalently by defined the spherical coordinates θ and ϕ as seen in Equation 1.

$$p_i = \begin{Bmatrix} \sin\theta\cos\phi \\ \sin\theta\sin\phi \\ \cos\theta \end{Bmatrix} \tag{1}$$

To consider complex material states, we consider N_p orientations or test fibers each with v_p volume fraction, and we introduce the superscript (n) to denote the nth orientation. Using this notation, we define volume averaging over the orientation state as orientation averaging and use the bracket operator $\langle\cdot\rangle$ as defined in Equation 2. Therefore, the commonly used second and fourth order orientation tensors are defined as $a_{ij} = \langle p_i p_j \rangle$ and $a_{ijkl} = \langle p_i p_j p_k p_l \rangle$.

$$\langle f \rangle = \sum_{n=1}^{N_p} v_p^{(n)} f^{(n)} \tag{2}$$

In this work, we explicitly store each orientation in contrast to the common practice of only using the second order orientation tensor. We perform fiber orientation update to an applied incremental deformation gradient, $F_{ij}^{\Delta t}$, as in Equation 3 representing affine fiber motion. Physically, this choice of orientation update method is motivated due to the limitation of independent motion of fibers at high aspect ratios and volume fraction. An approximation for the maximum mis-orientation angle of a single fiber in an array of aligned fibers is $\sin\theta \approx \left[\sqrt{\pi/V_f} - 2\right]\left[L_f/D_f\right]^{-1}$ where V_f is the fiber volume fraction and L_f/D_f is the fiber aspect ratio. Therefore, fibers with aspect ratio 100 are limited to a mis-orientation angle of 1° at $V_f = 22\%$, while fibers with aspect ratio 1,000 are limited to a mis-orientation angle of 1° at only $V_f = 0.8\%$. Hence, assuming fibers must reorient as the bulk fluid is a reasonable assumption for the regimes of interest.

$$p_i^{t+\Delta t} = F_{ij}^{\Delta t} p_j^t \Big/ \sqrt{F_{kl}^{\Delta t} F_{km}^{\Delta t} p_l^t p_m^t} \qquad [3]$$

Finally, we must consider a constitutive relationship which is dependent on this orientation state. We begin by considering a transversely isotropic, incompressible viscous compliance relationship as in Equation 4 where η_{11}, η_{22}, and η_{12} are the axial extensional viscosity, transverse extensional viscosity, and shear viscosity respectively, $\dot{\epsilon}_{ij}$ is the strain rate tensor, and σ_{ij} is the stress tensor. Micromechanics theories can be used for the determination of η_{11}, η_{22}, and η_{12} depending on fiber volume fraction, fiber aspect ratio, and the suspending polymer properties (Pipes, 1994). While rate dependent expressions for η_{11}, η_{22}, and η_{12} exist, we will consider the simplified case in which they are rate independent.

$$\begin{Bmatrix} \dot{\epsilon}_{11} \\ \dot{\epsilon}_{22} \\ \dot{\epsilon}_{33} \\ \dot{\gamma}_{23} \\ \dot{\gamma}_{13} \\ \dot{\gamma}_{12} \end{Bmatrix} = \begin{bmatrix} \frac{1}{\eta_{11}} & -\frac{1}{2\eta_{11}} & -\frac{1}{2\eta_{11}} & 0 & 0 & 0 \\ & \frac{1}{\eta_{22}} & \frac{1}{2}\left(\frac{\eta_{22}-2\eta_{11}}{\eta_{11}\eta_{22}}\right) & 0 & 0 & 0 \\ & & \frac{1}{\eta_{22}} & 0 & 0 & 0 \\ & & & \frac{4\eta_{11}-\eta_{22}}{\eta_{11}\eta_{22}} & 0 & 0 \\ & \text{sym.} & & & \frac{1}{\eta_{12}} & 0 \\ & & & & & \frac{1}{\eta_{12}} \end{bmatrix} \begin{Bmatrix} \sigma_{11} \\ \sigma_{22} \\ \sigma_{33} \\ \sigma_{23} \\ \sigma_{13} \\ \sigma_{12} \end{Bmatrix} \qquad [4]$$

As this relationship represents an incompressible material, the compliance relationship is singular as the resulting strain rate is independent of pressure. However, through the use of an appropriate pseudo inverse (Loredo, 1997), a deviatoric, viscous stiffness relationship can be determined. Additionally, the relationship can be orientation averaged (Advani, 1987) so that deviatoric stress is determined as a function of the orientation state and the applied strain rate, $\tau_{ij} = \langle\eta\rangle_{ijkl}\dot{\epsilon}_{kl}$. This final orientation averaged, rate independent, deviatoric stiffness tensor can be seen in Equation 5. As we have removed pressure from the constitutive relationship, we must determine pressure in an alternate manner. In Abaqus/Standard, hybrid formulation elements will be used, while in

Abaqus/Explicit, the incompressibility condition will be relaxed and a penalizing bulk modulus will be introduced.

$$\begin{aligned}\langle\eta\rangle_{ijkl} = 4\left[\frac{\eta_{11}^2}{4\eta_{11}-\eta_{22}} - \eta_{12}\right]\left(a_{ijkl}\right) + 4\left[\frac{\eta_{11}^2}{4\eta_{11}-\eta_{22}} - \frac{1}{3}\eta_{11}\right]\left(a_{ij}\delta_{kl} + a_{kl}\delta_{ij}\right) \\ + \left[\eta_{12} - \frac{\eta_{11}\eta_{22}}{4\eta_{11}-\eta_{22}}\right]\left(a_{ik}\delta_{jl} + a_{il}\delta_{jk} + a_{jl}\delta_{ik} + a_{jk}\delta_{il}\right) \\ +4\left[\frac{5}{18}\eta_{11} - \frac{\eta_{11}^2}{4\eta_{11}-\eta_{22}}\right]\left(\delta_{ij}\delta_{kl}\right) + \left[\frac{\eta_{11}\eta_{22}}{4\eta_{11}-\eta_{22}}\right]\left(\delta_{ik}\delta_{jl} + \delta_{il}\delta_{jk}\right)\end{aligned} \quad [5]$$

3. Implementation Details

To implement the presented model in Abaqus/Standard, a UMAT has been developed. As we will be using hybrid incompressible 3D elements, we are only required to define the deviatoric stress as well as the deviatoric, tangent stiffness matrix. The presented constitutive relationship takes the basic form of Equation 6. The best approximate for the strain rate from the inputs to the UMAT is $\dot{\epsilon}_{kl} = \Delta\epsilon_{kl}/\Delta t$. A natural location in the time interval to satisfy the constitutive relationship is then the midpoint (i.e. midpoint differencing). However, upon applying midpoint differencing, significant oscillations are seen in the resulting stress output due to jumps in strain rate which are common due to the displacement based formulation. To suppress these oscillations, we introduce a fading memory to the relationship through the use of regularization variables, $\xi_\tau, \xi_\eta \in [0, 1/2]$. Therefore, we make the substitutions $\tau_{ij} = \xi_\tau\tau_{ij}^0 + (1-\xi_\tau)\tau_{ij}^1$ and $\langle\eta\rangle_{ijkl} = \xi_\eta\langle\eta\rangle_{ijkl}^0 + \left(1-\xi_\eta\right)\langle\eta\rangle_{ijkl}^1$ into Equation 6 along with $\dot{\epsilon}_{kl} = \Delta\epsilon_{kl}/\Delta t$ to determine our stress update expression, Equation 7, where a superscript 0 indicates the beginning of the time increment and 1 indicates the end of the time increment. Equation 8 gives the resulting deviatoric tangent stiffness matrix.

$$\tau_{ij} = \langle\eta\rangle_{ijkl}\dot{\epsilon}_{kl} \quad [6]$$

$$\tau_{ij}^1 = \frac{1}{(1-\xi_\tau)\Delta t}\left[\xi_\eta\langle\eta\rangle_{ijkl}^0 + \left(1-\xi_\eta\right)\langle\eta\rangle_{ijkl}^1\right]:\Delta\epsilon_{kl} - \frac{\xi_\tau}{(1-\xi_\tau)}\tau_{ij}^0 \quad [7]$$

$$\frac{\partial\Delta\tau_{ij}}{\partial\Delta\epsilon_{kl}} = \frac{1}{(1-\xi_\tau)\Delta t}\left[\xi_\eta\langle\eta\rangle_{ijkl}^0 + \left(1-\xi_\eta\right)\langle\eta\rangle_{ijkl}^1\right] \quad [8]$$

We have assumed terms in Equation 8 coming from $\partial\langle\eta\rangle_{ijkl}/\partial\Delta\epsilon_{kl}$ are negligible compared to the retained terms. In application, for a general time step we set ξ_τ equal to ξ_η and both are set to a value greater than 0 and strictly less than $1/2$. In most cases, a value of 0.3 to 0.45 is sufficient to represent the intended constitutive relationship while allowing for a fading memory of the old stress term τ_{ij}^0. For an initial time step, we cannot assume that an initial stress of $\tau_{ij}^0 = 0$ is correct, nor can we be expected to determine the initial stress to appropriately prescribe to the model in general cases. Therefore, in the initial time increment, we set $\xi_\tau = 0$ and $\xi_\eta = 1/2$ effectively ignoring any initial stress state in the material. Additional calculations are performed by the UMAT, specifically, updating the fiber orientation state in response to incremental deformation as well as forming the orientation averaged stiffness tensors. Table 1 shows a pseudocode of the developed UMAT.

Table 1. UMAT Pseudocode

Let η_{11}, η_{22}, and η_{12} be input material properties.
Let τ_{ij}^0, ϵ_{ij}^0, F_{ij}^0, t^0, and $q_i^{(n)}$ be the fixed input deviatoric stress, strain, deformation gradient, time, and N_p orientations at the beginning of the current increment.
Let ϵ_{ij}^1, F_{ij}^1, and t^1 be the variable input (constant to UMAT, variable to solver) strain, deformation gradient, and time at the end of the current increment.
Compute viscous stiffness, $\langle\eta\rangle_{ijkl}^0$, using orientations, $q_i^{(n)}$.
Compute the incremental deformation gradient, $F_{ij}^\Delta = F_{ik}^1\left(F_{kj}^0\right)^{-1}$.
for $n = 1, 2, \ldots N_p$ (for each orientation)
    Compute and **store** the new orientation, $p_i^{(n)} = F_{ij}^\Delta q_i^{(n)} / \sqrt{F_{kl}^\Delta F_{km}^\Delta q_l^{(n)} q_m^{(n)}}$.
end for
Compute viscous stiffness, $\langle\eta\rangle_{ijkl}^1$, using orientations, $p_i^{(n)}$.
if $t_0 = 0$ and $\tau_{ij}^0 = \mathbf{0}$ **then** (if first increment and stress is not initialized)
    Compute and **store** the tangent stiffness matrix, $\partial\Delta\tau_{ij}/\partial\Delta\epsilon_{kl} = \left(\langle\eta\rangle_{ijkl}^0 + \langle\eta\rangle_{ijkl}^1\right)/(2\Delta t)$.
    Compute and **store** the new deviatoric stress, $\tau_{ij}^1 = \left(\partial\Delta\tau_{ij}/\partial\Delta\epsilon_{kl}\right)\Delta\epsilon_{kl}$.
else (no first increment or stress was initialized)
    Compute and **store** the tangent stiffness matrix, Equation 8.
    Compute and **store** the new deviatoric stress, Equation 7.
end if

Single element checks were performed for this UMAT. First, isolated strain rates were imposed on an element with a single orientation. However, the orientation update was disabled. Figure 1 shows an example of x_1 direction elongation applied with varying the strain rate. These results successfully matched the expected results. Another set of checks were performed with the orientation update enabled. In these cases, the fibers reorient in response to the loading and the resulting stress to a constant strain rate changes with respect to the total deformation. Figure 2 shows an example in which an element with a single fiber orientation initially aligned in the x_1 is shear in x_1-x_2 shear so that the fiber reorients toward the x_2 direction. Again, these checks were successful in replicating analytic solutions. A final set of checks were performed with multiple orientations per element. Figure 3 shows an example in which fibers are initially orientation in the x_1-x_2 plane with angle 0°, 60°, and $-60°$. The element was then subjected to plane strain extensional deformation in the x_1 direction. As can be seen the fibers reorient in response to the imposed deformation along with the stress response changing due to the reorientation matching analytic solutions.

Additionally, Figure 4 shows the response of the UMAT when regularization is not used versus when it is used. The applied strain is simple with two linear sections. However, these two linear sections of strain are equivalent to piecewise constant sections of strain rate. This jump in strain rate introduces oscillation as seen in the dotted curves that do not use regularization. With the use of regularization, the oscillation is damped out quickly as seen in the solid curve.

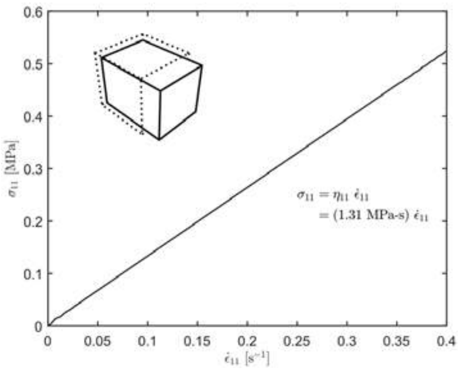

Figure 1. UMAT Single Element Check Example, Fiber Direction Elongation

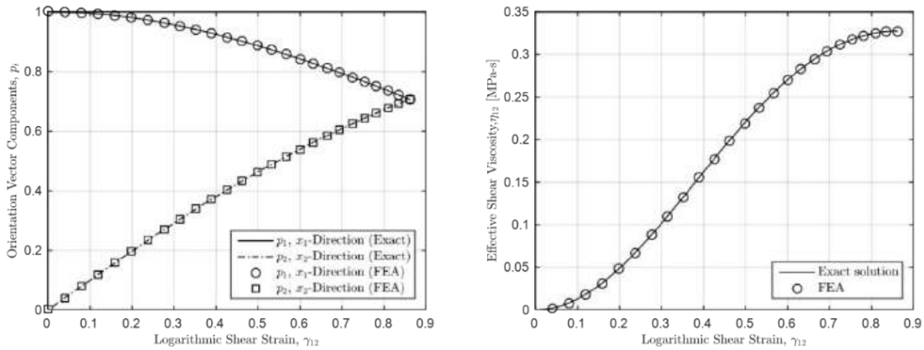

Figure 2. Simple Shear, Single Element with One Orientation Check
Orientation Components (left) and Effective Shear Viscosity (right) vs. Total Shear

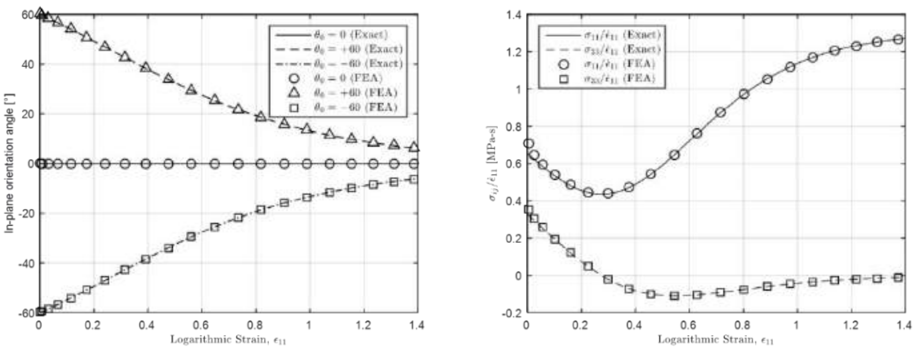

Figure 3. Plane Strain Elongation, Single Element with Multiple Orientations Check
Orientation Change (left) Stress to Strain Rate Ratios (right) vs. Total Extension

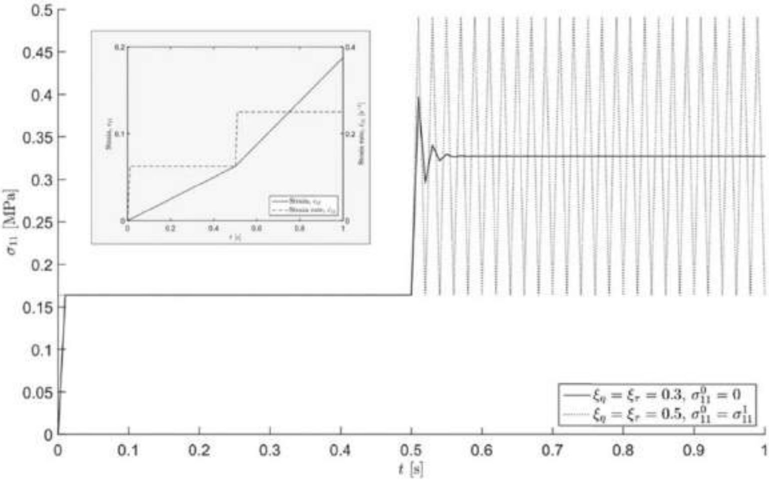

Figure 4. UMAT Regularization Check

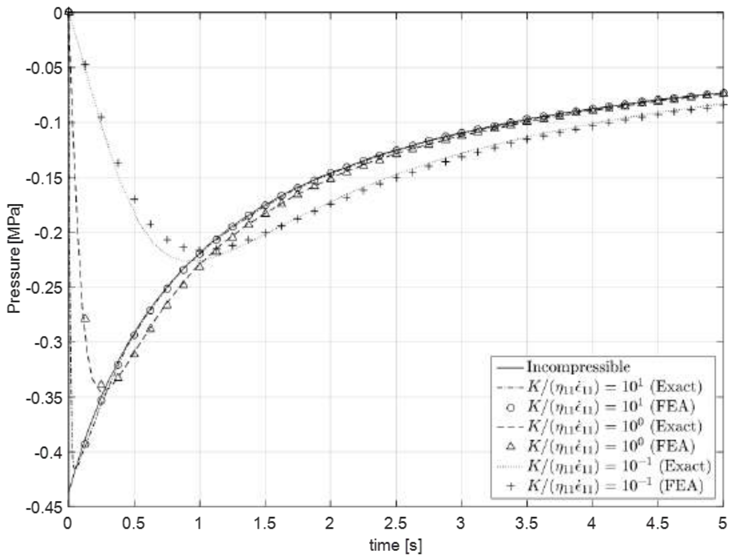

Figure 5. VUMAT Bulk Modulus Check, Pressure Comparison

Implementation in Abaqus/Explicit using a VUMAT is similar with the exception of returning a tangent stiffness matrix and the addition of pressure. As explicit time steps are much smaller than those possible in an implicit analysis, we make the simplification of setting $\xi_\tau = 0$ and $\xi_\eta = 1$ reducing the required computations per time step. Pressure is imposed through a penalizing bulk modulus giving $P^1 = -K\left[\det\left(F_{ij}^1\right) - 1\right]$ and $\sigma_{ij}^1 = \tau_{ij}^1 - P^1\delta_{ij}$.

Figure 5 shows the resulting pressure on a single element when different magnitudes of K are used. A simple rule of thumb this figured helps inform is that the bulk modulus should be approximately an order of magnitude larger than expected stress levels. For a certain material definition and applied strain rates this can be easily estimated or iterated. A final check in a model is to view the total volumetric strain present throughout the simulation.

4. Example: Squeeze Flow of a Circular Disk in /Standard

In order to apply and perform a first validation of this model, we investigate the simple case of squeeze flow with initial orientations that have a preferential direction. Ericsson et al. (Ericsson, 1997) investigated the effects of a coupled solution in this case along with experimental results for the diameter ratios of initially circular disks which deformed into elliptical shapes. Equation 9 shows their basic conclusion that the diameter ratio changes in response to squeezing based on the current orientation state.

$$\frac{dD_1}{dD_2} = \frac{D_1}{D_2}\frac{a_{2222}-a_{1122}}{a_{1111}-a_{1122}} \quad [9]$$

Initializing a model of a circular disk with orientation data equivalent to that measured and investigated by Ericsson et al., we determine diameter ratios through squeezing that can be seen in Figure 6 compared to Ericsson et al.'s experimental data as well as their simple analysis. In this case, fibers are initially oriented strongly in the x_1 direction. Therefore, this circles deform into elliptical disks with large x_2 diameter and small x_1 diameter. This simulation provides confidence in the presented model formulation and implementation.

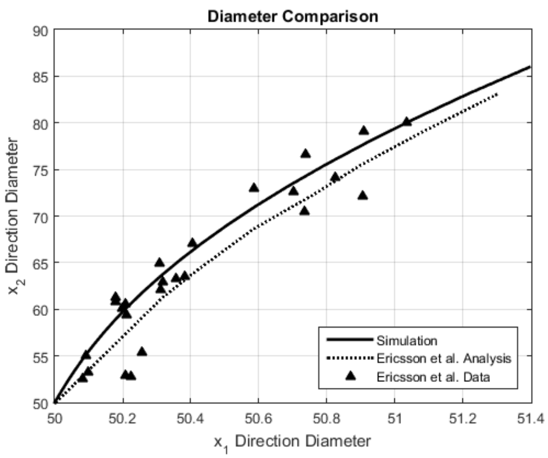

Figure 6. Diameter Ratio Simulation Results

5. Example: Center Gated Disk Flow in /Explicit using SPH

In order to further investigate the effect of anisotropy in flow, we consider the simple case of filling a center gated disk. Although the geometry is relatively simple (see Figure 6), flowing from a charge cavity into the final disk induces very large deformation requiring the use of Abaqus/Explicit and the smoothed particle hydrodynamics method. The charge is modeled as 92,378 PC3D elements. Orientations are initialized from several uniform random distributions in the x_1-x_2 plane with variable width. We consider three cases in which orientations are generated between $-\theta$ and θ: $\theta = 0.5°$, $\theta = 45°$, and $\theta = 90°$. Due to symmetry in the theory developed with respect to fiber orientations, $\theta = 90°$ represents fibers oriented throughout the entire x_1-x_2 plane although the angles used are only generated in the right half plane.

Figure 7 shows a bottom view of the relative velocity magnitude and current flow front position at 17% fill for the four cases considered. This fill point is before the anisotropic charges have encountered the boundary. Figure 8 shows the same view but at a time point once the anisotropic charges have encountered the boundary of the disk. Finally, Figure 9 shows the resulting orientation state for the four cases. From the figures it is clear that depending on the strength of the initial orientation, the stronger the eccentricity of the resulting deformation.

Looking specifically at the $\theta = 0.5°$ case, we can see that the flow changes from primarily x_2 direction extension to x_1-x_2 shear after encountering the boundary. This results in a large weld line along the x_1-x_3 plane. Clearly, effects are captured that cannot be captured in an uncoupled simulation, specifically drastically different final orientation state and potential defects.

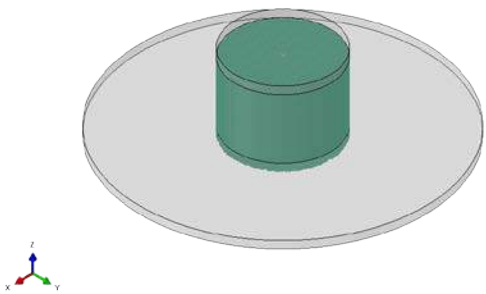

Figure 6. Center Gate Disk Geometry and Initial Charge (Green)

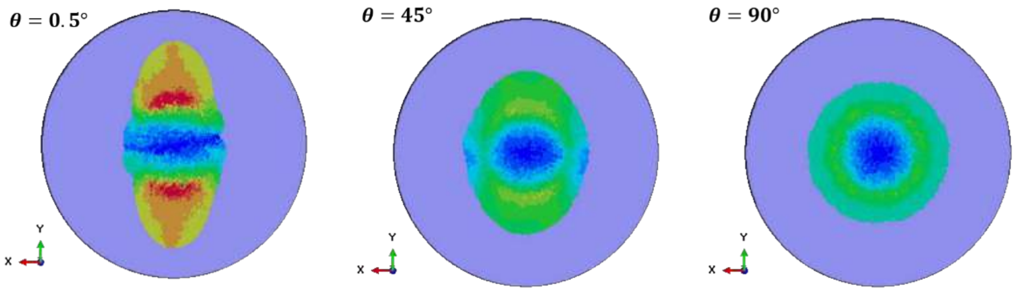

Figure 7. Bottom View of Velocity Magnitude and Flow Front Position at 17% Fill

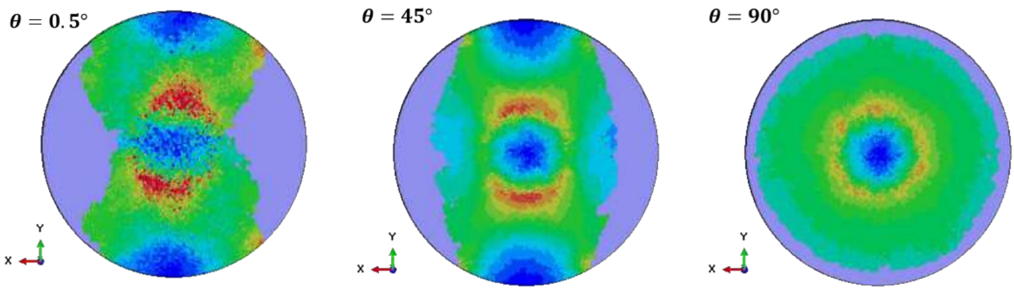

Figure 8. Bottom View of Velocity Magnitude and Flow Front Position at 63% Fill

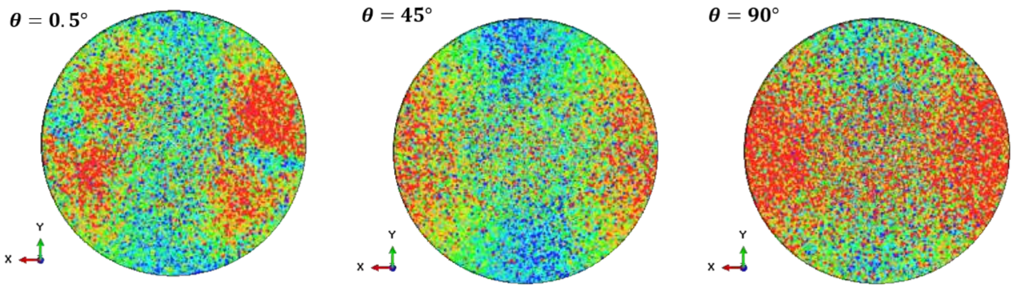

Figure 9. Bottom View of Orientation Component ($\mathbf{blue} = \mathbf{0} \leq |\boldsymbol{p_2}| \leq \mathbf{1} = \mathbf{red}$)

6. Conclusions

In this work, we have shown the method through which we are using Abaqus, both Abaqus/Standard and Abaqus/Explicit, to perform anisotropic viscous flow with fiber orientation analysis. This strongly coupled analysis is key to understanding the flow behavior of long fiber material systems which are used for both injection and compression molding. We have shown a validation test case in which squeeze flow (in /Standard) and center gated disk flow (in /Explicit) of initially strongly orientated charges are flowed from an initial shape of a circle into an elliptical shapes related to the strength of the initial orientation distributions. The squeeze flow case compared very well with available experimental data. This work heavily utilizes the flexibility of

Abaqus in terms of element choice, hybrid incompressible in /Standard and SPH in /Explicit, and user material definition implementation, UMAT and VUMAT.

7. Acknowledgements

This material is based upon work supported by the National Science Foundation Graduate Research Fellowship under Grant No. DGE-1333468.

8. References

1. Advani, S. G. and C. L. Tucker, "The Use of Tensors to Describe and Predict Fiber Orientation in Short Fiber Composites," *Journal of Rheology,* vol. 31, pp. 751-784, 1987.
2. Ericsson, K. A., S. Toll and J. A. Månson, "The two-way interaction between anisotropic flow and fiber orientation in squeeze flow," *Journal of Rheology,* vol. 41, pp. 491-511, 1997.
3. Folgar, F. and C. L. Tucker, "Orientation Behavior of Fibers in Concentrated Suspensions," *Journal of Reinforced Plastics and Composites,* vol. 3, pp. 98-119, 1984.
4. Jeffery, G. B., "The motion of ellipsoidal particles immersed in a viscous fluid," *Proceedings of the Royal Society A,* vol. 102, pp. 161-179, 1922.
5. Loredo, A. and H. Klöcker, "Generalized Inverse of the Compliance Tensor, and Behavior of Incompressible Anisotropic Materials - Application to Damage," *Mechanics Research Communications,* vol. 24, pp. 371-376, 1997.
6. Phelps, J. H. and C. L. Tucker, "An anisotropic rotary diffusion model for fiber orientation in short- and long-fiber thermoplastics," *Journal of Non-Newtonian Fluid Mechanics,* vol. 156, pp. 165-176, 2009.
7. Pipes, R. B., D. W. Coffin, P. Simacek, S. F. Shuler and R. K. Okine, "Rheological Behavior of Collimated Fiber Thermoplastic Composite Materials," in *Flow Phenomena in Polymeric Composites*, S. G. Advani and R. B. Pipes, Eds., Elsevier Science Publishers, 1994, pp. 85-125.
8. Tseng, H. C., R. Y. Chang and C. H. Hsu, "An objective tensor to predict anisotropic fiber orientation in concentrated suspension," *Journal of Rheology,* vol. 60, pp. 215-224, 2016.
9. Tucker, C. L., "Flow regimes for fiber suspensions in narrow gaps," *Journal of Non-Newtonian Fluid Mechanics,* vol. 39, pp. 239-268, 1991.